ACS APPLIED MATERIALS & INTERFACES

Research Article

www.acsami.org

High-Aspect-Ratio and Highly Ordered 15-nm Porous Alumina Templates

Jaime Martín, Cristina V. Manzano, Olga Caballero-Calero, and Marisol Martín-González*

IMM-Instituto de Microelectrónica de Madrid (CNM-CSIC), Isaac Newton 8, PTM, E-28760 Tres Cantos, Spain

Supporting Information

ABSTRACT: Ordered anodic aluminum oxide (AAO) templates with pores <15 nm in diameter and an aspect ratio (length-to-diameter ratio) above 3×10^3 have been fabricated using a nonlithographic approach; specifically, by anodizing aluminum in an ethylene-glycol-containing sulfuric acid electrolyte. The pores are the smallest in diameter reported for a self-ordered AAO without pore aspect-ratio limitations and good ordering, which opens up the possibility of obtaining nanowire arrays in the quantum confinement regime that is of interest for efficient thermoelectric generators. The effect of the ethylene glycol addition on both the pore diameter and the ordering is evaluated and discussed. Moreover, 15-nm-diameter Bi_2Te_3 and poly(3-hexyl thiophene) (P3HT) nanowires have been prepared using these AAO templates. As known, Bi_2Te_3 is currently the most efficient thermoelectric bulk material for room-temperature operations and, according with theory, its Seebeck coefficient should be increased when it is confined to nanowires with diameters close to 10 nm. On the other hand, P3HT is one of the main candidates for integrating organic photovoltaic and thermoelectric devices, and its properties are also proposed to increase when it is confined to nanoscale structures, mainly due to molecular orientation effects.

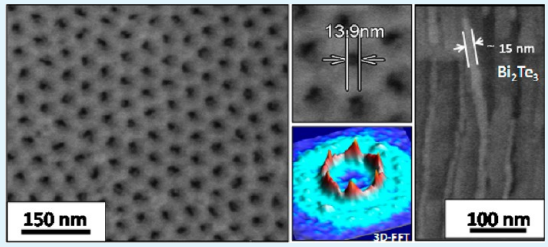

KEYWORDS: *alumina, arrays, porous materials, template synthesis, Bi_2Te_3, P3HT*

INTRODUCTION

Reducing the pore diameter of well-defined porous matrices is of great interest, from both technological and fundamental perspectives. For instance, diameters of a few nanometers are required for preparing efficient thermoelectric generators based on nanowire arrays.[1,2] Reduced pores are also crucial for catalysis and molecular sieving,[3] filtration,[4] reaching terabit magnetic information storage devices,[5] isolation of pathogens,[6] and so on. Moreover, they constitute ideal systems for investigating the size dependency of many chemical and physical properties.[7] Anodic aluminum oxide (AAO) is one of the most frequently used porous matrices for such purposes.

The template-based approach is a well-established method for the fabrication of nanostructures in a variety of materials.[8−15] AAO also stands out as an efficient template, thanks to its well-defined pore geometry and high tunability over its characteristic features, namely, pore diameter, pore length, interpore distance (D_{int}), and pore density (ρ_p). For example, pores ranging from 20 nm to 400 nm in diameter have been reported in the literature for AAO templates.[16−19] These characteristics, along with the closed-hexagonal arrangement of its pores, make the AAO a promising candidate for the development of different types of devices, including thermoelectric generators. In general, there are several requirements that a template should fulfill for its efficient integration in nanodevices:

(i) Pores should present ultralow diameters, allowing the achievement of nanostructures that present quantum confinement effects. Given thef act that these effects are often visible exclusively for structures of only tens of nanometers, these are the diameters of the templates we are targeting.[1,20]

(ii) It muat be possible to fabricate high-aspect-ratio pores. This is necessary for applications such as thermoelectric generators, where nanowires of several tens of micrometers in length are needed in order to avoid thermal percolation. Furthermore, mechanically stable templates are often required for the synthesis of the nanowires, which, from a practical point of view, implies the need for large pore lengths (>20 μm).

(iii) Finally, periodically organized pores are preferred, since the more ordered the template is, the less dispersion in diameter size is obtained.

In this sense, Gösele's team reported on the fabrication of a self-ordered AAO with pores ∼20 nm in diameter via a two-step anodization.[16] To the author's knowledge, it represents the state-of-the-art lowest diameter for a self-ordered AAO without aspect-ratio limitations and ordered pore arrangement. On the other hand, Masuda et al. obtained pores below 20 nm by different approaches.[16−18] However, because of the fact that the conditions used for the second anodizations are far from the self-ordering conditions, it is difficult to achieve high-aspect-ratio pores by those approaches, since the pore arrangement order will be lost as pores grow in length. Moreover, those

Received: September 26, 2012
Accepted: December 6, 2012
Published: December 6, 2012

   dx.doi.org/10.1021/am3020718 | ACS Appl. Mater. Interfaces 2013, 5, 72−79

anodizations were performed in highly concentrated sulfuric acid at high temperature, so the AAO pore walls would be hardly attacked during the large anodization times required for having high aspect-ratio pores (see Figure S1 in the Supporting Information). Taking all of these into account, the diameter limit that is currently well-established in the literature for high-aspect-ratio pores is 20 nm. Therefore, the objective of this work is to reduce the pore diameter of the ordered alumina templates while maintaining a high-aspect-ratio coefficient. For that, our strategy is based on two initial concepts.

The first consideration is that the applied voltage (V) controls both the pore diameter (d_p) and the cell size (interpore distance, D_{int}). However, while the latter seems to be almost exclusively related to the applied voltage V,[21] the pore diameter, d_p, is susceptible to being affected by other variables, such as the electric field strength (E) at the growth front between alumina and the solution.[22] Consequently, a general approach to reduce d_p might be modifying the d_p/D_{int} ratio while keeping D_{int} constant. That is, to increase E while maintaining V at a constant value. This is related to the models established by Su et al. in a series of recent papers, which explain, among other important aspects of anodic layers, the pore morphology, the self-ordering, and the pore initiation.[23−27] Furthermore, they determined that the d_p/D_{int} ratio is directly governed by the relative dissociation rate of the water supplying of oxygen anions to the oxide/metal interface. Hence, the d_p/D_{int} ratio could be tailored through the variables that affect such dissociation rates,[24] namely, V, E, etc. In this sense, Chen et al. recently claimed to have modulated the d_p/D_{int} ratio by means of increasing E by reducing the dielectric constant (ε) of a phosphoric acid solution.[28] Thus, the addition of an organic compound, such as ethylene glycol, to the acidic electrolyte solution will modify ε. Ethylene glycol has a lower dielectric constant ($\varepsilon_{ethylene\ glycol}$ = 41.1 at 20 °C) than water (ε_{water} = 72 at 20 °C). Moreover, it is completely soluble in the aqueous electrolyte, and it can be added up to high concentrations.

The second concept is that some organic compounds tend to protect the AAO pore walls from the dissolution in an acidic electrolyte.[28] In the case of anodizations carried out in sulfuric acid solutions, the dissolution of the pore walls is especially significant. While the porosity values (volume fraction occupied by pores) of the AAOs obtained in oxalic and phosphoric acid solutions are <10%,[17,29] the porosity of the AAO obtained in 0.3 M sulfuric acid, under 25 V, is ∼12%,[29] and for AAO obtained in 20 wt % sulfuric acid, under 19 V, is 14%.[16] These last conditions for anodizations in sulfhuric acid are known to lead to the smallest diameter pore ordered AAOs with high aspect ratio (also see Figure S2 in the Supporting Information). Those porosity values indicate a strong dissolution of the AAO pore walls in the sulfuric acid solutions, when compared with the porous alumina obtained in oxalic or phosphoric acid solutions.

Based on these two ideas, we propose the use of a mixture of sulfuric acid, water, and ethylene glycol to anodize aluminum. Under these conditions, ordered AAO <15 nm in diameter and with large-aspect-ratio pores (3×10^3) have been obtained for the first time. The pore diameters of these AAO templates are the smallest reported for an ordered AAO without limitations on pore aspect ratio. Thus, the templates are suitable for preparing ordered arrays of one-dimensional (1D) quantum nanostructures, which means a significant advance toward quantum devices. Moreover, in order to demonstrate the usability of the obtained porous alumina templates, 15 nm in diameter and ultrahigh-aspect-ratio Bi_2Te_3 and poly(3-hexyl thiophene) (P3HT) nanowires have been prepared. Devices based on arrays of nanowires composed of these materials should be highly interesting for thermoelectric and photovoltaic applications. On the one hand, Bi_2Te_3 and derived alloys are the most efficient thermoelectric bulk materials at a working temperature of 25 °C and low-dimensional nanostructures composed thereof are attracting considerable interest, because of the promise that quantum confinement will increase their efficiencies.[1] On the other hand, P3HT is currently attracting notable interest for a variety of energetic applications, including photovoltaic cells and thermoelectric devices.[30,31] The preparation methods have been eletcrodeposition[9−11] and capillary infiltration of the molten polymer,[8,32] respectively.

EXPERIMENTAL SECTION

Preparation of the AAO Templates. Ordered AAO templates have been prepared by a two-step electrochemical anodization of aluminum.[18] To begin with, ultrapure (99.999%) aluminum foils (Advent Research Materials, England), were cleaned and degreased by sonication in acetone, water, isopropanol, and ethanol. Foils were then electropolished in a solution of perchloric acid/ethanol (1/3) under a constant voltage of 20 V, and after that, the first anodization was achieved for 24 h. A 10 wt % sulfuric acid (Panreac AC Química, Spain) solution was used as electrolyte for all the samples. The applied voltage (V) was 19 V, and the reaction temperature was 0 °C. The appropriate amount of ethylene glycol (Panreac AC Química, Spain) was also added to the sulfuric acid solution in such a way that the final ethylene glycol concentrations were: 0, 10, 40, 50, 60, 75, and 90 wt %. The first anodic layer then was removed by chemical etching in a mixture of phosphoric acid (7 wt %) and chromic oxide (1.8 wt %). Finally, the second anodization was performed in the same conditions as the first one but for 16 h, unless specified otherwise.

Characterization. The morphology of AAOs was performed by scanning electron microscopy (SEM) (Hitachi, Model SU8000) operating at an accelerating voltage of 0.5 kV to avoid the deposit of any conducting layer and charging. The microscope had been properly calibrated by the operators from Hitachi, Ltd. Also, the accuracy of the measurement was checked in the 20- and 25-nm alumina templates reported in the Figure S2 in the Supporting Information. For the cross-sectional SEM images, the Al substrates were dissolved in an acid solution of $CuCl_2$, and then, the AAOs were fractured in order to examine the pores along their longitudinal direction. The Fourier transforms (FTs) of the SEM images were calculated using scanning probe image software (WSxM 3.1).[33] The dispersion of the pore sizes was calculated using laboratory-developed software. The Raman scattering of the AAO samples was measured using a LabRam HR Raman spectrometer (Horiba Jobin−Yvon) with a 532-nm wavelength Nd:YAG laser (8.5 mW) in the range between 350 and 1250 cm^{-1}, in air and at room temperature. The P3HT was analyzed using a 632.8-nm wavelength (10 mW) He−Ne laser in the range between 600 cm^{-1} and 2000 cm^{-1}, also in air and at room temperature. Finally, a Philips X'Pert four-circle diffractometer system was used for the X-ray diffraction (XRD) experiments.

P3HT and Bi_2Te_3 Nanowire Array Preparation. For the template-based fabrication of the P3HT nanowires, commercially available regioregular P3HT (>95% regioregular, Aldrich, Ltd.) was infiltrated into the nanopores by capillary action.[34] The experiment was performed placing a P3HT film onto the AAO and annealed at 260 °C under N_2 atmosphere for 1 h, and then the temperature was decreased at 1 °C/min down to room temperature. In the case of Bi_2Te_3, it was electrodeposited into the AAO template using a similar procedure to the one described in refs 9 and 11. A potentiostat-galvanostat (Eco Chemie, Model AUT302.0) was used for electrodeposition of the 15 nm Bi_2Te_3 nanowires.

dx.doi.org/10.1021/am3020718 | ACS Appl. Mater. Interfaces 2013, 5, 72−79

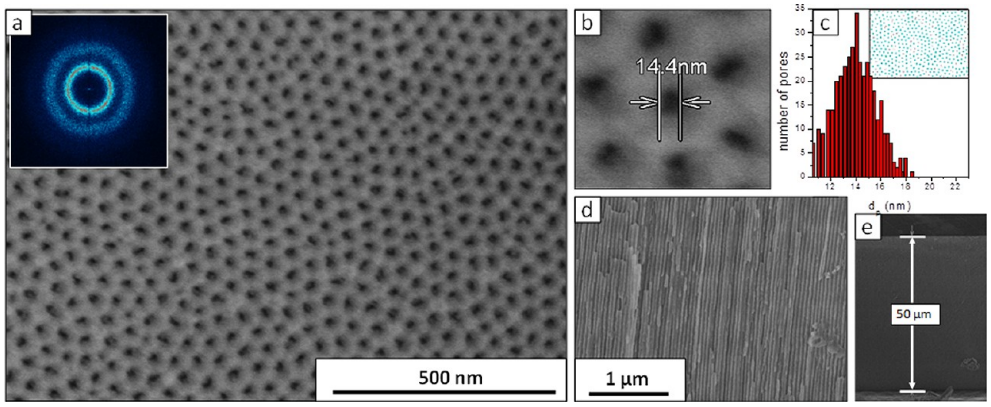

Figure 1. SEM micrographs of the AAO anodized in the presence of 50 wt % of ethylene glycol. (a) Large view where the polydomain structure can be seen (magnification: 100 000×); the inset corresponds to the Fourier transform (FT) of an image taken at 50 000×. (b) High-magnification SEM micrograph of the hexagonal cell from which the pore diameter has been directly measured. (c) Pore diameter distribution diagram obtained from the digitally analyzed image shown in the inset. (d) Detailed view of the cross section where the parallel pore walls can be clearly seen. (e) Total thickness of one of the templates (~50 μm).

Table 1. Characteristic Features of the Obtained AAO Templates

ethylene glycol [wt %]	pore diameter, D_p [nm]	interpore distance, D_{int} [nm]	porosity, P [%]	pore density, ρ [pore/cm^2]	growth rate, v [μm/h]	final regularity parameter, R_f
0	19	50	14.1	4.6×10^{10}	4.3	319
10	18	50	11.9	4.6×10^{10}	3.9	983
40	18	50	11.9	4.6×10^{10}	2.1	1279
50	14	50	7.1	4.6×10^{10}	0.7	1463
60	15	50	8.2	4.6×10^{10}	0.7	1021
75	16	50	9.5	4.6×10^{10}	0.2	825
90						

RESULTS AND DISCUSSION

Figure 1a shows a typical large-view SEM micrograph of the AAO template anodized for 16 h. It can be seen that the pores are organized according to a closed-packed hexagonal symmetry within ordered domains. These domains, in turn, are randomly oriented, as can be deduced from the FT shown in the inset of Figure 1a. The pore diameter (d_p) was measured both directly (from a high-magnification SEM image; see Figure 1b) and by means of the digital analysis of a SEM image (Figure 1c). Both measurements arouse a diameter value of ~14 nm. It should be noted that, since the contrast of the SEM image depends on the observation conditions, such as the magnification value, we measured the pore diameter of the obtained AAO templates through SEM images acquired at different magnifications, and the same diameter value was obtained (see Figures S3a and S3b in the Supporting Information). Furthermore, the same diameter values were also obtained when cross-sectional SEM mages were analyzed (see Figure S3c in the Supporting Information). In this work, the AAOs are prepared using the same mild conditions in the first and second anodizations. Thus, we avoid the loss of order which would be the consequence of using different electrolytes in each anodization. Moreover, as such conditions are "soft", the electrolyte does not damage the pore structure upon pore growth during the second anodization. So, completely parallel pores can be obtained, as it can be seen in the cross section shown in the SEM image of Figure 1d, which were obtained after the fracture of the AAO to see the longitudinal directions of the pores. Furthermore, the pores maintain their ordered distribution after 16 h of second anodization, as evidenced in the SEM images of the bottom surface of the AAO, that is, the surface of the barrier layer (see Figure S3d in the Supporting Information). It is also worth noting that the D_{int} is again 50 nm in this region. These two points additionally confirm that the pores do not collapse during their growth in length and that their walls are completely parallel. This point is further confirmed in the cross-sectional SEM micrograph shown in Figure 1d. Taking all of these into account, one can conclude that the pores maintain their structural quality independent of their length; that is, this AAO does not present limitations on its pore aspect ratio. Thus, a 50-μm-thick AAO template was prepared, which is shown in the large cross-sectional view of Figure 1e. This proves that pores with aspect ratios above 3300 have been obtained. It is important to highlight here that the obtained templates, to the best of our knowledge, are the smallest pore diameters achieved for an ordered porous alumina with nonlimited pore lengths.

As far as the porosity of the AAOs is concerned, a D_{int} value of 50 nm has been measured. This value implies a D_{int}/V ratio of 2.6 nm/V, which is almost equal to that obtained for other anodizations carried out under self-ordering reaction conditions in the mild anodization regime (2.5 nm/V).[35] This fact also demonstrates that a reduction of the ε on the electrolyte due to the addition of ethylene glycol does not affect to D_{int}, which was one of the ideas upon which our strategy was based. The measured D_{int} value leads to a calculated pore density of 4.6×10^{10} pores/cm^2. From the relationship between d_p and D_{int}, one can calculate the porosity of the material.[29] Thus, a value of 7.1% was obtained, which is considerably lower than the typical porosity values of the AAO templates anodized under self-ordering conditions, using sulfuric acid as an electrolyte: The porosity of the AAO obtained in 0.3 M sulfuric acid under 25 V

dx.doi.org/10.1021/am3020718 | ACS Appl. Mater. Interfaces 2013, 5, 72−79

is 12%, as reported elsewhere,[29] or 11%, according to our results (see Figures S2a, S2b, and S2c, as well as Table S1 in the Supporting Information); however, that of the AAO obtained in 20 wt % sulfuric acid under 19 V is 14%, as reported elsewhere,[16] or 19%, according to our results (see Figures S2g, S2h, and S2i, as well as Table S1 in the Supporting Information). The low porosity obtained in our new AAOs could be attributed to the presence of ethylene glycol. On the one hand, according to Chen et al.,[28] and indirectly also to Su et al.,[23−27] the lower ε of the electrolyte seems to induce a lower (d_p/D_{int}) ratio, through the increase of the electric field strength and the consequent enhancement of the water dissociation rate at the pore bottom. On the other hand, the organic compound seems to have a protecting effect against the pore wall dissolution, preventing the pores from widening.[21] Thus, pore widening cannot be appreciated in the AAO template, even after 70 h of anodization (see Figure S4 in the Supporting Information).

In order to further evaluate the effect of the ethylene glycol on the obtained AAO, different ethylene glycol concentrations (0, 10, 40, 50, 60, 75, and 90 wt %) were used (Table 1). Figure 2 shows the current density versus time (j−t) transients for

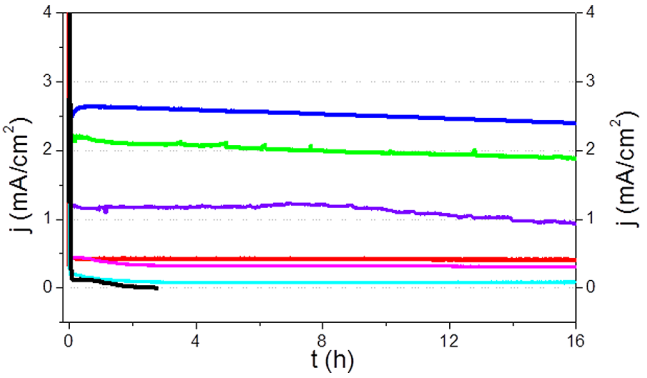

Figure 2. Current density−time transients during the second anodizations in 0, 10, 40, 50, 60, 75, and 90 wt % ethylene glycol and 10 wt % H_2SO_4. The curve for the anodizations performed in 90 wt % ethylene glycol and 10 wt % H_2SO_4 corresponds to the first anodization.

second anodizations, except for the 90 wt % ethylene-glycol-containing electrolyte, for which the first anodization is shown. This was due to the rapid stop of the reaction in the 90 wt % ethylene-glycol-containing electrolyte, where the current density dropped to zero within <3 h, as can be seen in Figure 2. This is due to a lack of oxygen ions in the electrolyte, which comes mostly from water oxidation, according with the reaction

$$2H_2O(l) \rightarrow O + 2H^+(aq) + 2e^-$$

This highlights the importance of water in anodizations.

We measured the thicknesses of the AAOs anodized for 16 h, and from those values, the growth rates were calculated. The thickness and growth rate values were 70 and 4.3 μm/h for the AAO anodized in the absence of ethylene glycol; 62 and 3.9 μm/h for the AAO anodized in the presence of 10 wt % ethylene glycol; 33 and 2.1 μm/h for the AAO anodized in the presence of 40 wt % ethylene glycol, 12 and 0.7 μm/h for the AAO anodized in the presence of 50 wt % ethylene glycol, 11 and 0.7 μm/h for the AAO anodized in the presence of 60 wt % ethylene glycol, and 3.8 and 0.2 μm/h for the AAO anodized in the presence of 75 wt % ethylene glycol. (see Table 1 and Figure 3). The thicknesses were measured from the SEM images of the cross sections, as shown in Figure S5 in the

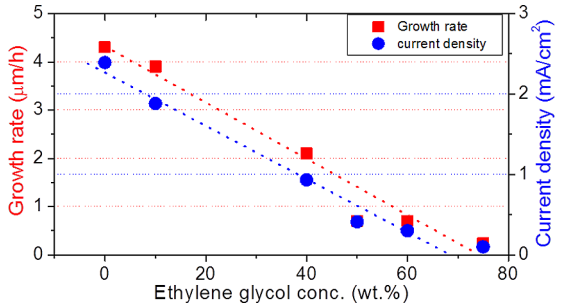

Figure 3. Plot of the growth rate (v) and plateau current density (j) constant value against ethylene glycol concentration.

Supporting Information. Thus, an almost-linear dependence of the growth rate on the ethylene glycol concentration (in wt %) was found (Figure 3). Equally, a linear dependence of the steady-state current density on the ethylene glycol was observed. The steady-state current densities were extracted from the current density values at 16 h of anodization.

Figures 4a−c show the surface views of the AAO templates obtained using 0, 10, 40, 50, 60, and 75 wt % of ethylene glycol. The diameter values of those AAOs were, 19, 18, 18, 14, 15, and 16 nm, respectively. Therefore, in general, smaller pore diameters were measured as the ethylene glycol concentration was increased (Figure 4 (insets) and Table 1), the smallest being those obtained in the sample anodized in 50-wt %-ethylene-glycol-containing electrolyte. In contrast, the interpore distance (D_{int}) is 50 nm for the three samples, which evidence that the ethylene glycol has a direct effect on the pore diameter d_p or on the porosity, P, but not on the D_{int}. Figures 4d, 4e, and 4f show the schematic illustrations, done to scale, of the d_p to D_{int} relationship for the three samples. Moreover, the consequences of the partial dissolution of the AAO in the electrolyte can be clearly observed in the surface of the AAO obtained in the absence of ethylene glycol (Figure 4a). Those consequences are the widening of pores and the partial dissolution of the inert part of the AAO pore walls also at the AAO surface, which leads to the formation of sharp convex angles between the pores. Such effects are not present in the AAO anodized in the presence of the organic compound and are usually indicative of the high solubility of the AAO in the electrolyte. Furthermore, an enhancement of the apparent pore ordering while increasing the ethylene glycol concentration can be also observed. While the ordered domains are hardly distinguishable in the AAO anodized in the absence of ethylene glycol (Figure 4a), ordered domains over distances of 300−500 nm are present in the AAO anodized with 50 wt % ethylene glycol (Figure 4c). In order to perform a semi-quantitative analysis of the regularity of the pore array, we calculated a regularity parameter (R) from the three-dimensional (3D) FT of the SEM micrographs, following the method proposed by Sulka et al.[36] (Figure 5a, 5c, 5e, 5g, 5i, and 5k). R was defined as the ratio of the intensity to the full-width-at-half-maximum (I_p/fwhm) of the FT intensity profile. In this way, R is closely related to the regularity of the nanostructure. For the six samples, the FTs show an intensity ring corresponding to the random orientation of the first neighboring pores. Moreover, for the AAO obtained in 50 wt % ethylene glycol, a second concentric ring can be also observed, corresponding to

dx.doi.org/10.1021/am3020718 | ACS Appl. Mater. Interfaces 2013, 5, 72−79

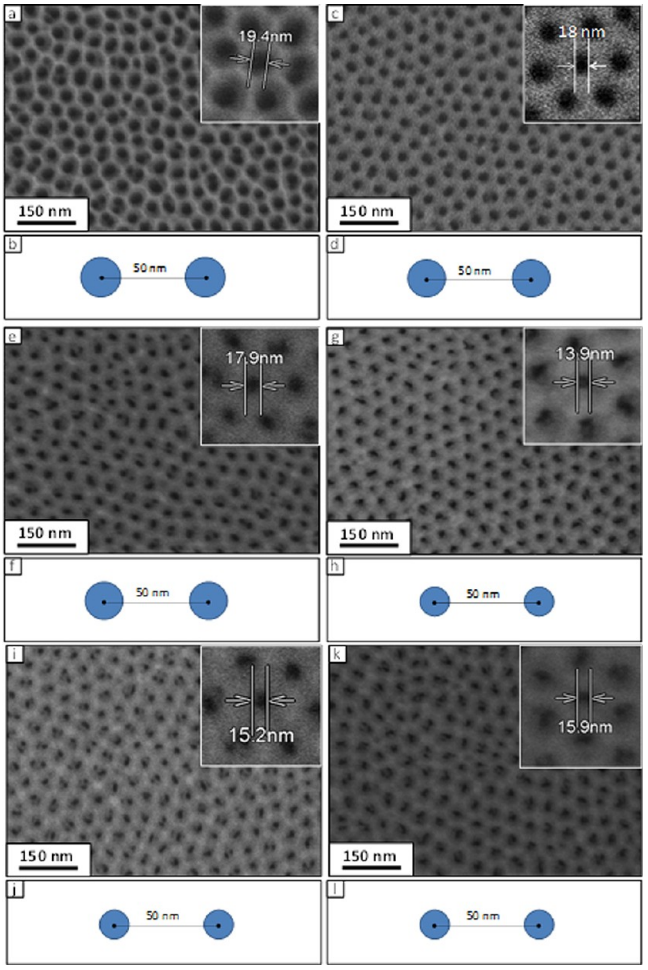

Figure 4. (a, c, e, g, i, k) SEM micrographs of the AAOs anodized in the presence of 0, 10, 40, 50, 60, and 75 wt % ethylene glycol, respectively. The insets show enlarged views of the hexagonal cells, where the pore diameter have been measured. (b, d, f, h, j, l) Schematic illustrations of the $d_p - D_{int}$ relationship of the samples.

the second neighboring pores. The final regularity parameter (R_f) was calculated by averaging the R values of six intensity peaks obtained from three profiles with different orientations, such as those shown in Figure S6 of the Supporting Information. The corresponding intensity profiles are presented in Figures 5b, 5d, 5f, 5h, 5j, and 5l. Thus, the R_f values collected in Table 1 were obtained. The R_f values of the AAO anodized in 0, 10, 40, 50, 60, and 75 wt % ethylene glycol were 319, 983, 1279, 1463, 1021, and 825, respectively. A clear increase in R_f is observed as the ethylene glycol concentration increases for AAO with the same first anodization times (24 h in all cases). Thus, the pore ordering is related to the presence of ethylene glycol, in such a way that the most ordered structure was obtained for the sample that was anodized in a 50-wt %-ethylene-glycol-containing electrolyte.

For comparison, we also calculated the R_f value of the reported state-of-the-art AAOs.[16,19] The R_f value for the AAO ~20 nm in pore diameter (obtained in 20 wt % sulfuric acid under 19 V) was 827 (see Figures 2j, 2k, and 2l in the Supporting Information). This R_f value is considerably lower than that of these new AAO templates (R_f = 1463), demonstrating that this new AAO presents a higher degree of order, in addition to lower diameter pores, compared to the state-of-the-art lowest-diameter-pore AAO. In contrast, the R_f value obtained for the AAO with 25-nm-diameter pores (0.3 M sulfuric acid and 25 V) was 27111 (see Figures S2d, S2e, and S2f in the Supporting Information), which evidence the higher pore ordering of the template obtained under such conditions.

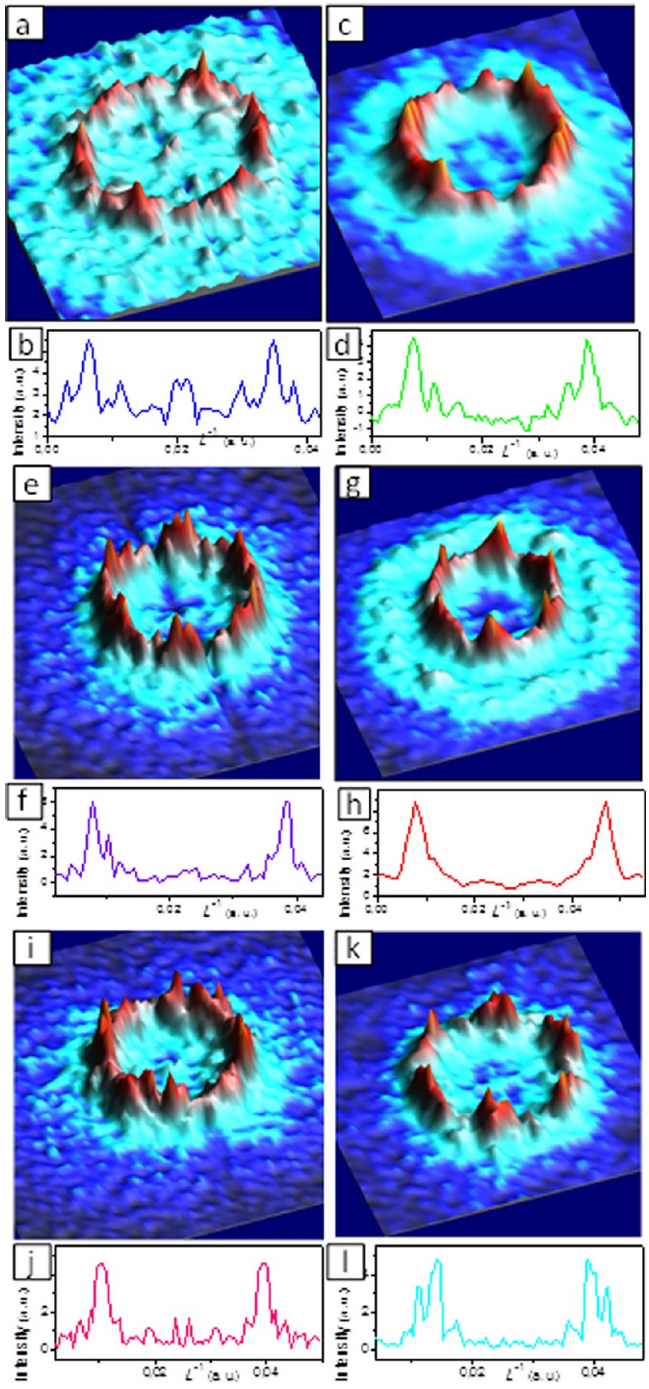

Figure 5. (a, c, e, g, i, k) Three-dimensional (3D) Fourier transformation (FT) of the SEM images of the AAOs anodized in the presence 0, 10, 40, 50, 60, and 75 wt.% ethylene glycol, respectively. (shown in Figure 4). (b, d, f, h, j, l) FT intensity profiles of AAOs anodized in the presence of 0, 10, 40, 50, 60, and 75 wt % ethylene glycol, used afterward for the calculation of the regularity parameter (R).

In order to know whether ethylene glycol induced any compositional variations in the AAO that could explain the observed improvement, high-resolution Raman spectroscopy measurements were performed on the AAOs prepared in the

dx.doi.org/10.1021/am3020718 | ACS Appl. Mater. Interfaces 2013, 5, 72−79

absence and presence (50 wt %) of ethylene glycol (Figure 6). These results rule out a possible incorporation of ethylene

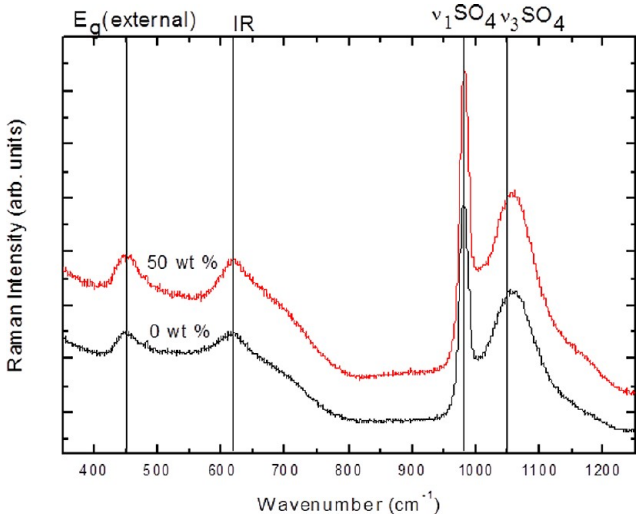

Figure 6. Raman spectra of the AAO anodized in 0 and 50 wt % ethylene glycol and 10 wt % H_2SO_4.

glycol molecules into the structure of the AAO. The Raman spectra of both samples are similar, showing five bands located at the same wavenumber values: 451, 615, 981, and 1056 cm^{-1}. The band at 451 cm^{-1} corresponds to E_g (external) mode, while the band at 615 cm^{-1} is attributed to infrared (IR) active modes.[37] The intense bands at 981 cm^{-1} and 1056 cm^{-1} are assigned to the υ_1 band and to the $\upsilon\upsilon_3$ band of the SO_4 group in aluminum sulfate, respectively.[38] Therefore, in both cases, SO_4^{2-} ions are incorporated into the alumina pore walls in the same way, so both AAOs present the same composition, independenty of being synthesized in the presence or absence of ethylene glycol. Similarly, the internal structures of both AAOs were identical, as was also determined by X-ray diffraction (see Figure S7 in the Supporting Information).

It is also important to emphasize here that the obtained AAO are mechanically stable when removed from the aluminum substrate. This enables their use not only as closed-end-pore templates, but also as through-hole membranes after the removal of the barrier layer. Thus, these membranes can be used for the electrodeposition of nanowire arrays or for applications where a through-hole membrane is required, such as nanofiltration, molecular delivery, etc.

In order to demonstrate the usability of these sub-15-nm-diameter nanoporous templates, nanowires of the thermoelectric Bi_2Te_3 and semiconducting polymer P3HT have been prepared using two different techniques: electrodeposition in the first case and melt capillary infiltration in the second case. Figure 7a shows a cross-section of prepared 15-nm-diameter

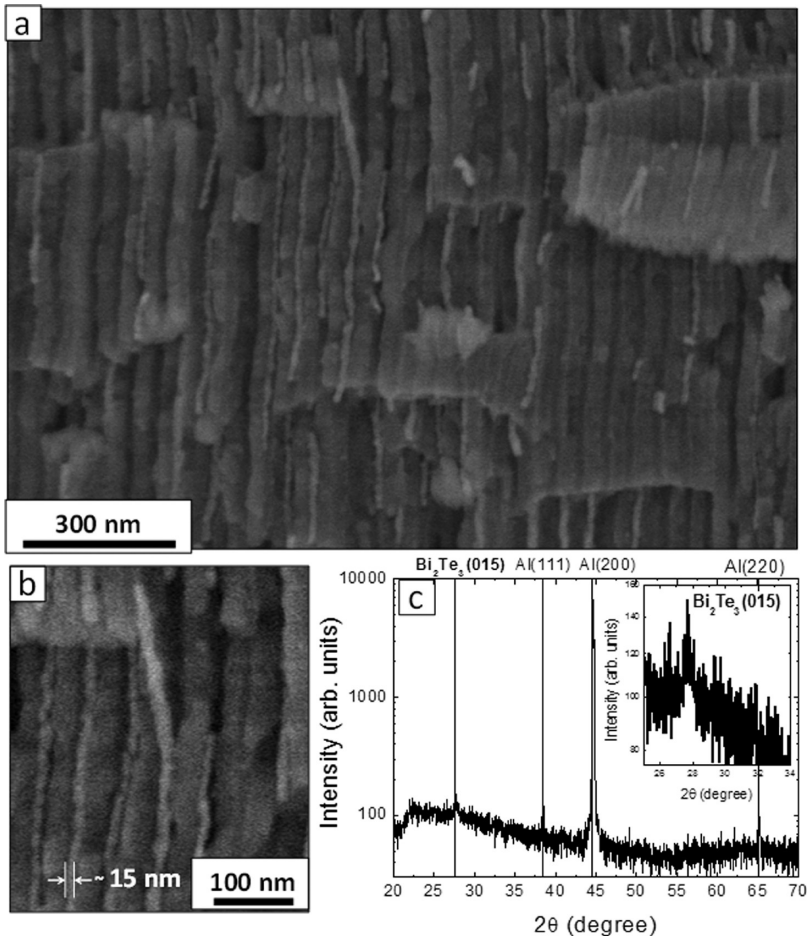

Figure 7. (a and b) SEM images of cross section of 15-nm Bi_2Te_3 nanowires located inside the AAO nanopores. The composition of the nanowires is demonstrated by XRD diffraction (c), where the main diffraction peak of the Bi_2Te_3 crystal can be observed. The inset shows an enlarged view of the diffraction.

dx.doi.org/10.1021/am3020718 | ACS Appl. Mater. Interfaces 2013, 5, 72−79

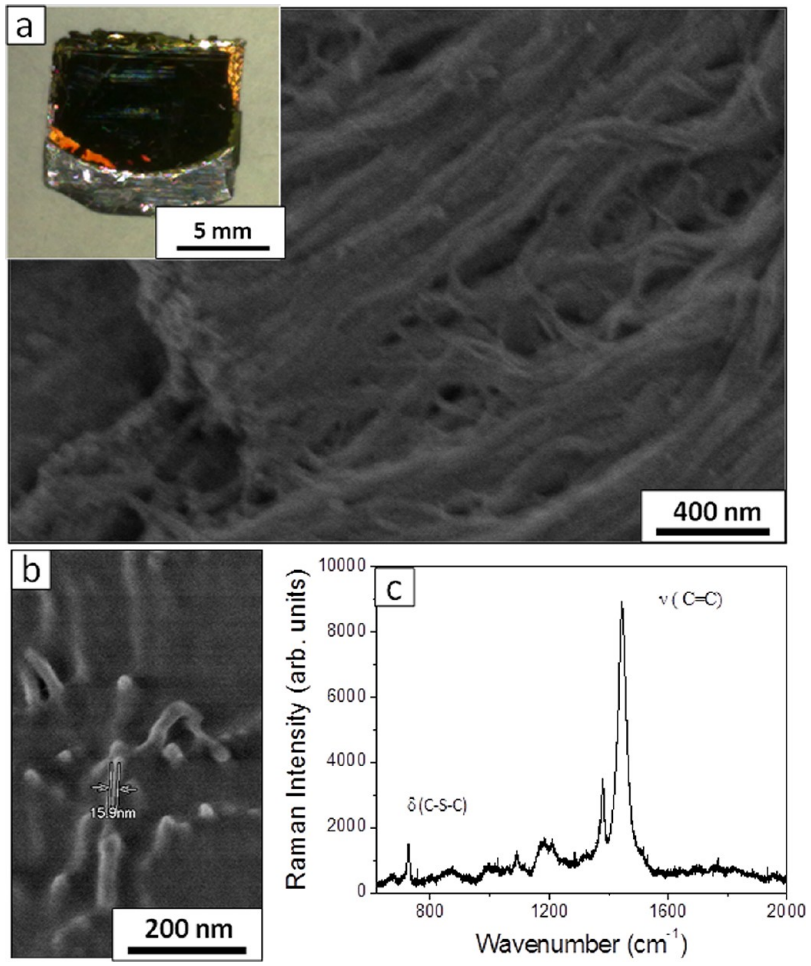

Figure 8. (a) SEM micrographs of the P3HT nanowires after the removal of the AAO template; the inset shows a photograph of the P3HT-containing AAO template. (b) Cross-sectional SEM image of a 15-nm-diameter AAO template filled with P3HT. (c) Raman spectrum of P3HT nanowires embedded in the AAO template.

Bi_2Te_3 nanowires located inside the AAO nanopores after the fracture of the template, while Figure 7b shows a detailed view of a Bi_2Te_3 nanowire, where its reduced diameter is demonstrated. The Bi_2Te_3 nanowires are broken as a consequence of the fracture of the template. The XRD pattern performed to the ensemble of nanowires (Figure 7c) presents the reflection associated to the (015) Bi_2Te_3 crystal, which is typically the strongest diffraction line of the Bi_2Te_3 pattern (see Figure S8 and Table S2 in the Supporting Information). The rest of the diffraction peaks are due to the Al substrate. The inset shows an enlarged view of the diffraction peak. On the other hand, Figure 8a shows the bundles of P3HT nanowires after being extracted from the template by the selective dissolution of the AAO. The nanowires laid down and collapsed, because of their high aspect ratios and the capillarity forces that appear during the evaporation of the rinsing water used after the dissolution of the AAO. The inset shows a photograph of the AAO template filled with P3HT. Figure 8b shows the cross-sectional image of a 15-nm-diameter AAO templates filled with P3HT. At some points, the P3HT nanowires can be seen protruding from the pores. Figure 8c shows the Raman spectrum of the P3HT nanowires. The Raman band at 728 cm^{-1} is assigned to the deformation vibration of the C−S−C bond, while the intensive bands at 1442 and 1380 cm^{-1} can be attributed to the C═C stretching vibrations of the thiophene ring and the skeletal stretching, respectively.[39]

■ CONCLUSIONS

In this contribution, we report, for the first time, on an ordered anodic aluminum oxide (AAO) <15 nm in diameter and with a large aspect ratio by anodizing in an aqueous electrolyte composed of 10 wt % sulfhuric acid and 50 wt % ethylene glycol. In order to get this result, a study of the dependence of the different parameters of the AAOs with the addition of different concentrations of ethylene glycol was performed. It was found that the pore diameter decreases as the ethylene glycol concentration is increased, while the pore ordering is enhanced with the addition of ethylene glycol. Under the optimal conditions, pores with the smallest diameter values reported to date for an AAO without limitation on pore aspect-ratio were prepared. This new AAO allows one to prepare ordered arrays of high-aspect-ratio one-dimensional (1D) quantum nanostructures that could be integrated in quantum devices. As an example of their usability, nanowires 15 nm in diameter composed of Bi_2Te_3 and poly(3-hexyl thiophene) (P3HT) have been prepared and characterized

dx.doi.org/10.1021/am3020718 | ACS Appl. Mater. Interfaces 2013, 5, 72−79

■ ASSOCIATED CONTENT

Supporting Information

Extensive SEM micrographs and image analysis of the obtained AAO as well of those of the state-of-the-art AAOs. X-ray diffraction (XRD) measurements of the samples. XRD data and pattern of Bi_2Te_3 obtained from the Inorganic Crystal Structure Database. This information is available free of charge via Internet at http://pubs.acs.org/.

■ AUTHOR INFORMATION

Corresponding Author

*E-mail: marisol@imm.cnm.csic.es.

Notes

The authors declare no competing financial interest.

■ ACKNOWLEDGMENTS

Authors want to thank the ERC 2008 Starting Grant "Nano-TEC" (No. 240497). C.V.M. and O.C.C. acknowledge CSIC and European Union Funding for a JAE Ph.D. grant and a JAE postdoctoral position, respectively.

■ REFERENCES

(1) Hicks, L. D.; Dresselhaus, M. S. *Phys. Rev. B* **1993**, *47*, 12727−12731.
(2) Nielsch, K.; Bachmann, J.; Kimling, J.; Böttner, H. *Adv. Energy Mater.* **2011**, *1*, 713−731.
(3) Corma, A. *Chem. Rev.* **1997**, *97*, 2373−2420.
(4) Yamaguchi, A.; Uejo, F.; Yoda, T.; Uchida, T.; Tanamura, Y.; Yamashita, T.; Teramae, N. *Nat. Mater.* **2004**, *3*, 337−341.
(5) Juang, J.-Y.; Bogy, D. *Microsyst. Technol.* **2005**, *11*, 950−957.
(6) Yang, S. Y.; Ryu, I.; Kim, H. Y.; Kim, J. K.; Jang, S. K.; Russell, T. P. *Adv. Mater.* **2006**, *18*, 709−712.
(7) Martín, J.; Krutyeva, M.; Monkenbusch, M.; Arbe, A.; Allgaier, J.; Radulescu, A.; Falus, P.; Maiz, J.; Mijangos, C.; Colmenero, J.; Richter, D. *Phys. Rev. Lett.* **2010**, *104*, 197801.
(8) Martín, J.; Maiz, J.; Sacristan, J.; Mijangos, C. *Polymer* **2012**, *53*, 1149−1166.
(9) Martín-González, M.; Prieto, A. L.; Gronsky, R.; Sands, T.; Stacy, A. M. *Adv. Mater.* **2003**, *15*, 1003−1006.
(10) Martín-González, M.; Prieto, A. L.; Knox, M. S.; Gronsky, R.; Sands, T.; Stacy, A. M. *Chem. Mater.* **2003**, *15*, 1676−1681.
(11) Martín-González, M.; Snyder, G. J.; Prieto, A. L.; Gronsky, R.; Sands, T.; Stacy, A. M. *Nano Lett.* **2003**, *3*, 973−977.
(12) Liu, H.; Li, Y.; Jiang, L.; Luo, H.; Xiao, S.; Fang, H.; Li, H.; Zhu, D.; Yu, D.; Xu, J.; Xiang, B. *J. .Am. Chem. Soc.* **2002**, *124*, 13370−13371.
(13) Liu, H.; Xu, J.; Li, Y.; Li, Y. *Acc. Chem. Res.* **2010**, *43*, 1496−1508.
(14) Guo, Y.; Tang, Q.; Liu, H.; Zhang, Y.; Li, Y.; Hu, W.; Wang, S.; Zhu, D. *J. Am. Chem. Soc.* **2008**, *130*, 9198−9199.
(15) Zheng, H.; Li, Y.; Liu, H.; Yin, X.; Li, Y. *Chem. Soc. Rev.* **2011**, *40*, 4506−4524.
(16) Jessensky, O.; Muller, F.; Gosele, U. *Appl. Phys. Lett.* **1998**, *72*, 1173−1175.
(17) Martín, J.; Manzano, C. V.; Martín-González, M. *Microporous Mesoporous Mater.* **2012**, *151*, 311−316.
(18) Masuda, H.; Fukuda, K. *Science* **1995**, *268*, 1466−1468.
(19) Masuda, H.; Hasegwa, F.; Ono, S. *J. Electrochem. Soc.* **1997**, *144*, L127−L130.
(20) Mingo, N. *Appl. Phys. Lett.* **2004**, *84*, 2652−2654.
(21) Parkhutik, V. P.; Shershulsky, V. I. *J. Phys. D: Appl. Phys.* **1992**, *25*, 1258.
(22) Ono, S.; Saito, M.; Ishiguro, M.; Asoh, H. *J. . Electrochem. Soc.* **2004**, *151*, B473−B478.
(23) Su, Z.; Bühl, M.; Zhou, W. *J. Am. Chem. Soc.* **2009**, *131*, 8697−8702.
(24) Su, Z.; Hahner, G.; Zhou, W. *J. Mater. Chem.* **2008**, *18*, 5787−5795.
(25) Su, Z.; Zhou, W. *Adv. Mater.* **2008**, *20*, 3663−3667.
(26) Su, Z.; Zhou, W. *J. Mater. Chem.* **2011**, *21*, 357−362.
(27) Su, Z.; Zhou, W.; Jiang, F.; Hong, M. *J. Mater. Chem.* **2012**, *22*, 535−544.
(28) Chen, W.; Wu, J.-S.; Xia, X.-H. *ACS Nano* **2008**, *2*, 959−965.
(29) Nielsch, K.; Choi, J.; Schwirn, K.; Wehrspohn, R. B.; Gösele, U. *Nano Lett.* **2002**, *2*, 677−680.
(30) Xuan, Y.; Liu, X.; Desbief, S.; Lecl; egrave; re, P.; Fahlman, M.; Lazzaroni, R.; Berggren, M.; Cornil, J.; Emin, D.; Crispin, X. *Phys. Rev. B* **2010**, *82*, 115454.
(31) Vohra, V.; Campoy-Quiles, M.; Garriga, M.; Murata, H. *J. Mater. Chem.* **2012**, *22*, 20017−20025.
(32) Steinhart, M. *Adv. Polym. Sci.* **2008**, 123−187.
(33) Horcas, I.; Fernandez, R.; Gomez-Rodriguez, J. M.; Colchero, J.; Gomez-Herrero, J.; Baro, A. M. *Rev. Sci. Instrum.* **2007**, *78*, 013705.
(34) Moon, S. I.; McCarthy, T. J. *Macromolecules* **2003**, *36*, 4253−4255.
(35) Lee, W.; Ji, R.; Gosele, U.; Nielsch, K. *Nat. Mater.* **2006**, *5*, 741−747.
(36) Sulka, G. D. Chapter 1: Highly Ordered Anodic Porous Alumina Formation by Self-Organized Anodizing. In *Nanostructured Materials in Electrochemistry*; Wiley−VCH Verlag GmbH & Co. KGaA: Weinheim, Germany, 2008; pp 1−116. (DOI: 10.1002/9783527621507.ch1.)
(37) Li, D.; Jiang, C.; Ren, X.; Long, M.; Jiang, J. *Mater. Lett.* **2008**, *62*, 3228−3231.
(38) Kloprogge, J. T.; Frost, R. L. *J. Mater. Sci.* **1999**, *34*, 4199−4202.
(39) Baibarac, M.; Lapkowski, M.; Pron, A.; Lefrant, S.; Baltog, I. *J. Raman Spectrosc.* **1998**, *29*, 825−832.